



Rotating ring-disk electrode as a quantitative tool for the investigation of the oxygen evolution reaction



Ivan S. Filimonenkov^{a, b, *}, Sergey Ya. Istomin^a, Evgeny V. Antipov^a, Galina A. Tsirlina^a, Elena R. Savinova^b

^a Department of Electrochemistry, Faculty of Chemistry, Lomonosov Moscow State University, 1/3 Leninskie Gory, 119991 Moscow, Russia

^b ICPEES, UMR 7515 du CNRS-ECPM, 25 rue Becquerel, 67087 Strasbourg Cedex 2, France

ARTICLE INFO

Article history:

Received 18 June 2018

Received in revised form

13 August 2018

Accepted 13 August 2018

Available online 14 August 2018

Keywords:

Rotating ring-disk electrode (RRDE)

Oxygen evolution reaction (OER)

Faradaic efficiency

Catalyst loading

Carbon corrosion

ABSTRACT

In this work we analyze the applicability limits of the rotating ring-disk electrode (RRDE) technique for quantifying the amount of oxygen produced during the oxygen evolution reaction (OER). We utilize a state-of-the-art IrO₂ oxide as a carbon-free OER catalyst and La_{1-x}Sr_xMn_{0.5}Co_{0.5}O_{3-δ}, x = 0.25 and 0.5 perovskites, which are studied in the presence of carbon. RRDE experiments are performed at different IrO₂ loadings under both potentiodynamic and potentiostatic modes. The experimental data allow us to formulate the requirements to the experimental conditions necessary to avoid underestimation of the oxygen yield.

© 2018 Elsevier Ltd. All rights reserved.

1. Introduction

Water electrolysis occupies an important place in the electrochemical energy conversion and storage [1]. The choice of active and sufficiently stable electrode materials for the anodic OER is the most complex problem of the water electrolysis [2–4]. For the proton-exchange membrane water electrolysis the materials choice is largely reduced to Ir-based anodes, other materials not being capable of sustaining the acidic medium at high anodic potentials [5]. Last decades have evidenced significant increase in the interest towards water electrolysis in liquid and solid alkaline electrolysis cells, whereby various transition metal oxides have been investigated regarding their OER activity [1–3]. Many of transition metal oxides are rather poor electron conductors urging their utilization in combination with conductive binders, carbon materials currently being the most widely employed [3,6–8]. At high anodic potentials carbon corrosion is unavoidable and occurs simultaneously with the OER. Thus, accurate measurements of the OER activities of oxides studied in the presence of carbon additives require

determination of the OER current efficiency [3].

Various techniques have been suggested for quantifying the amount of the evolved oxygen, including fluorescence oxygen sensors [9,10], differential and online mass spectrometry [11–16], scanning electrochemical mass spectrometry [17,18]. The rotating ring-disc electrode (RRDE), whereby oxygen evolved at a disk electrode is detected at the ring, is characterized by a low detection limit, does not require special cell development, and thus seems to be a convenient method for determining the OER efficiency of oxide/carbon composite electrodes. Surprisingly, the RRDE method is rarely applied to studies of the OER. Even for carbon-free electrodes the reported OER current efficiencies range from 100% [19,20] to much lower values [21–24] suggesting possible instrumental complications.

High catalyst loadings on the disc electrode appear to be one of the current explanations for the apparent low OER efficiencies whereby the pores of a catalytic layer might be blocked by oxygen bubbles under the conditions of the oxygen evolution. However, the loading effect seems to be a matter of controversy: some publications documented a decrease [20,25–29], while the other an independence [27,30] or even an increase of the OER specific activity with the loading [25].

The objective of this work is to explore the applicability and eventual limitations of the RRDE as a quantitative method for the

* Corresponding author. Department of Electrochemistry, Faculty of Chemistry, Lomonosov Moscow State University, 1/3 Leninskie Gory, 119991 Moscow, Russia.

E-mail addresses: filimonenkov@elch.chem.msu.ru, ivan.filimonenkov@etu.unistra.fr (I.S. Filimonenkov).

OER investigation. In order to do so we apply a carbon-free IrO₂ OER catalyst, which is investigated in a wide range of loadings (from 5 to 400 μg cm⁻²) both under potentiodynamic and under potentiostatic conditions. We then test two non-noble oxides (Co- and Mn-containing perovskites La_{1-x}Sr_xMn_{0.5}Co_{0.5}O_{3-δ}, x = 0.25, 0.5) with a carbon binder to quantify the OER efficiency under the conditions of the simultaneous oxygen evolution and carbon corrosion.

2. Experimental

2.1. Synthesis of the iridium oxide powder

IrO₂ powder was obtained by thermal oxidation of unsupported metallic Ir nanoparticles of ca. 2 nm diameter synthesized by direct reduction of an anhydrous Ir salt in water-free conditions as described in Ref. [31]. The oxidation was performed at 490 °C in a furnace under air by using a heating rate of 5 °C min⁻¹ and a dwell time of 0.5 h as specified in Ref. [32]. This procedure resulted in the formation of rod-shape IrO₂ particles with a mean width of ca. 5.5 nm and a length of ca. 15.0 nm and rutile crystalline structure as described in Ref. [33]. Specific surface area of the IrO₂ sample was estimated from TEM measurements neglecting particle agglomeration as ca. 74 m² g⁻¹.

La_{1-x}Sr_xMn_{0.5}Co_{0.5}O_{3-δ}, x = 0.25 and 0.5 perovskites with 10.2 and 5.7 m² g⁻¹ BET surface areas, respectively, were prepared by modified Pechini method. In this method, for the preparation of 3 g of samples, stoichiometric amounts of Mn(CH₃COO)₂·3.8H₂O, Co(NO₃)₂·5.38H₂O and La(NO₃)₃·5.25H₂O (all analytical grade, exact water content of the salts was determined from thermogravimetric analysis in air) were dissolved in 50 ml of distilled water where the solution prepared by dissolution of SrCO₃ in a minimum volume of concentrated HNO₃ was added. The obtained solution was transferred in a porcelain cup into which a solution of 24 g of diammonium citrate in 30 ml of water was added. Final pH of the resulting solution was adjusted to 7 by the addition of HNO₃ (conc) or NH₃ (aq) whereupon 5 g of acrylamide (Acros Organics, 98.5%) and 1.02 g of N,N'-methylenebisacrylamide (Acros Organics, 96%) were added. The solution was heated at a ceramic plate until a transparent gel was formed. The resulting gel was first annealed in air at 450 °C for 2 h, then at 800 °C for 6 h, ground and finally treated at 900 °C for 12 h. The phase purity of the prepared perovskites was checked by their X-ray powder diffraction (XRPD) patterns (Fig. S1) recorded with a Huber G670 Image plate Guinier diffractometer (CuKα₁ radiation, curved Ge monochromator, image plate detector). According to scanning electron microscopy (SEM) images obtained with Carl Zeiss NVision 40 microscope operated at 1–20 kV, the samples contain sintered particles with the size 20–50 nm (Fig. S2).

2.2. Electrode preparation

For electrochemical measurements the IrO₂ catalyst was deposited from IrO₂/water suspensions (0.03–2.6 mg ml⁻¹ depending on the desired loading) onto a glassy carbon (GC) disk electrode mirror-like polished using alumina/water pastes with the 1, 0.3 and 0.05 μm alumina particle size. IrO₂ loadings per cm² of the geometric surface area ranged from 5 to 400 μg cm⁻². For the preparation of the 91 and 400 μg cm⁻² loadings certain portions of IrO₂ were mixed with the calculated amounts of pure water (18.2 MΩ cm, <1 ppb TOC, Purelab) followed by the treatment in the ultrasound bath (ca. 10 min). In case of 5, 15 and 45 μg cm⁻² loadings the ink prepared for the 91 μg cm⁻² loading was diluted with calculated amounts of pure water. To obtain distributed and reproducible catalyst layers, three 10 μl portions of the ink were

subsequently drop-cast onto the GC disk using a micropipette, with and intermediate drying under a slow N₂ gas stream. At the final stage, 6 μl portion of an alkaline ionomer AS4 (Tokuyama Company) aqueous solution was dropped onto the deposited catalyst layer and dried under N₂, to provide the ionomer content of 1.3 μg cm⁻². The electrochemical tests with bare (catalyst-free) GC disk electrode were also performed in the presence of ionomer for the sake of comparison.

La_{1-x}Sr_xMn_{0.5}Co_{0.5}O_{3-δ}, x = 0.25 and 0.5 perovskites were mixed (1:1 on the weight basis) with a pyrolytic carbon of the Sibunit family [34] with 82 m² g⁻¹ BET surface area. These mixtures were used for preparing aqueous suspensions and deposited on the GC disk electrode as specified in Ref. [35] to attain carbon and perovskite loadings of 15 μg cm⁻².

2.3. Electrochemical measurements

Electrochemical measurements were performed in a three-electrode Teflon cell with the upper part made of Pyrex glass. 1 M NaOH solution was prepared from the 50 wt% NaOH aqueous solution (Sigma-Aldrich). The working electrode was a RRDE with a GC disk (5 mm diameter) and gold ring (7.5 mm outer diameter and 6.5 mm inner diameter) equipped with a MSR rotator system, both from Pine Research Inst. The counter electrode was a smooth Pt wire and the reference electrode was a Hg/HgO electrode filled with 1 M NaOH. All potentials reported below were recalculated into the scale of the reversible hydrogen electrode (RHE): $E_{\text{RHE}} = E_{\text{Hg/HgO}/1\text{ M NaOH}} + 0.930\text{ V}$. Measurements were made using an Autolab bipotentiostat-galvanostat PGSTAT302N equipped with a linear scan generator module. The temperature of the cell was kept at 25 °C using a water-cooled thermostatic bath. The cell resistance was determined from a high-frequency intercept of electrochemical impedance hodographs (see Fig. S3 in the Supplementary information) recorded for all loadings at OER potentials in the 0.1 Hz to 100 kHz frequency range with an amplitude of 5 mV. The estimated resistance values ranged from 45 to 55 Ohm.

All cyclic voltammograms (CVs) of the disk electrode were recorded at a 10 mV s⁻¹ scan rate. The RRDE collection efficiency (24.9% at 900 rpm) was determined from the ring and disk current ratios in 1 M NaOH + 10 mM K₃[Fe(CN)₆] solution (Fig. S4). The ring potential (+0.3 V vs. RHE) for RRDE studies of the OER was chosen based on the oxygen reduction reaction (ORR) voltammograms recorded on the Au ring in the O₂-saturated 1 M NaOH solution (Fig. S5). Before RRDE measurements the gold surface of the ring electrode was cleaned by applying 100 potential cycles in the interval from 0.03 to 1.53 V at 200 mV s⁻¹.

3. Results and discussion

3.1. Electrochemical characterization of the IrO₂ catalyst

To check whether the RRDE is applicable in a wide range of the catalyst loadings it is important to first make sure that the catalyst surface is fully accessible. Thus, CVs of the IrO₂ catalyst were recorded in a narrow potential window from 0.93 to 1.03 V (Fig. 1a) where neither the OER nor the ORR interferes with the measurements, and the electrode shows pseudo-capacitive currents. After subtraction of the background GC current and normalization of CVs to the catalyst loadings, the curves for various loadings merge within the accuracy of 9% (Fig. S6), confirming the surface accessibility in the interval of the catalyst loadings applied. The error is the highest for the lowest loading in this series because the subtracted GC background is comparable with the catalyst response. The CV for the highest loading demonstrates a small ohmic distortion. The anodic and cathodic charge values extracted from

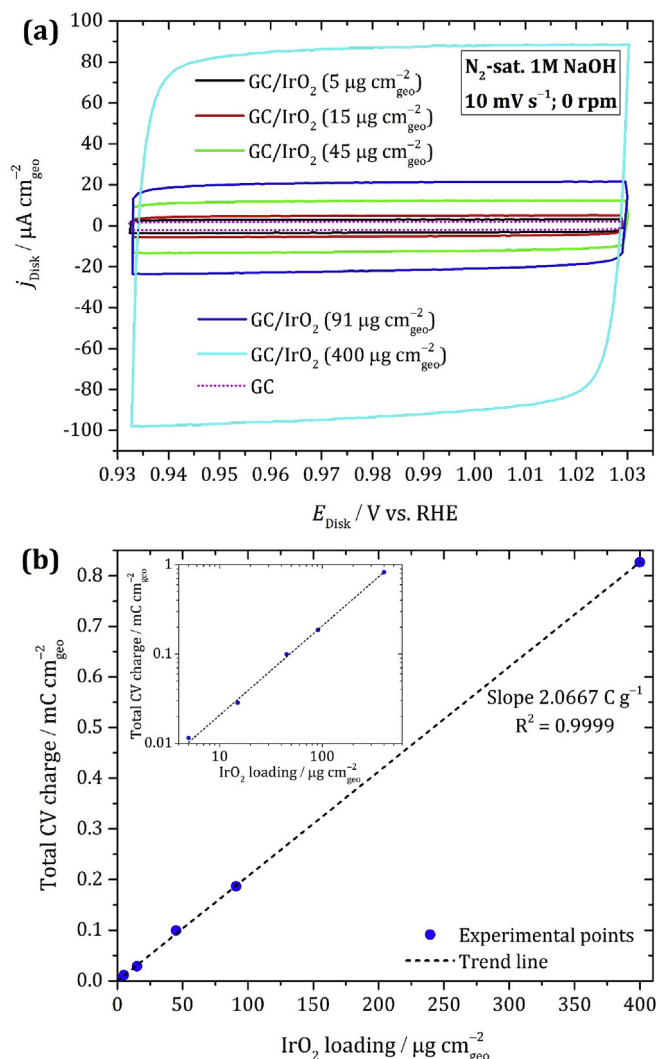


Fig. 1. (a) CVs of GC-supported IrO₂ catalyst in the interval 0.93–1.03 V at 10 mV s⁻¹ in N₂-saturated 1 M NaOH for various catalyst loadings. (b) Average voltammetric charges extracted from corresponding CVs at various IrO₂ loadings after GC correction. The inset represents this figure in the bilogarithmic scale.

this series of CVs (Fig. 1a) are collected in Table S1, and their average absolute values are plotted in Fig. 1b. The latter demonstrate linear dependence on the loading with the slope of ca. 2.1 C g⁻¹ that corresponds to mass-weighted capacity of 21 F g⁻¹ and specific capacity of 0.03 mF cm⁻²_{TEM}. A comparable value (ca. 40–80 F g⁻¹) was observed for thermally prepared IrO₂ in 1 M NaOH in Ref. [36]. In contrast, much higher capacity of ca. 266 F g⁻¹ or 0.82 mF cm⁻²_{BET} was observed for IrO₂ in 1 M KOH in Ref. [20]. Note that the capacity of thermally prepared IrO₂ was shown to depend on its degree of crystallinity [37].

Fig. 2 shows the CVs of the IrO₂ catalyst with various loadings for a wider (0.43–1.43 V) potential window, with the broad peaks corresponding to the reversible Ir(III)/Ir(IV) redox transition [20,36]. The shape of these CVs is in good agreement with the literature data for thermally prepared IrO₂ (which demonstrates some differences as compared to an electrochemically formed IrO₂) [36,38,39]. Oxygen traces could not be removed completely from the RRDE cell, and minor contribution of the ORR is noticeable at potentials below 0.8 V. For the highest loading, when this trace contribution is minimal, the background-corrected cathodic and

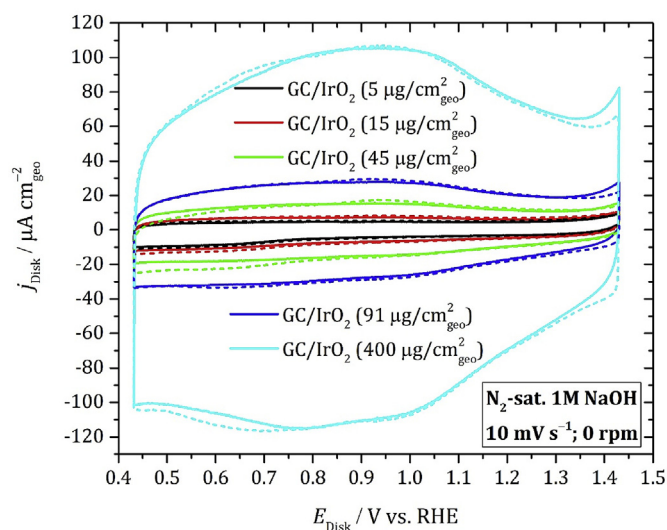


Fig. 2. CVs of GC-supported IrO₂ catalyst in the interval 0.43–1.43 V at 10 mV s⁻¹ in N₂-saturated 1 M NaOH for various catalyst loadings acquired before (solid lines) and after (dashed lines) the OER.

anodic charges are equal to 8.5 and 8.4 mC cm⁻² respectively, and the mean polarization capacity corresponds to ca. 21 F g⁻¹ in agreement with the above-mentioned value.

The negligible difference of CVs registered after (dashed curves) and before (solid curves) OER experiments (Fig. 3) confirms stability of IrO₂ during the OER within the applied experimental conditions.

3.2. RRDE investigation of the oxygen evolution on the IrO₂ catalyst

*i*r-corrected RRDE curves in the potential interval of the OER are shown in Fig. 3 for various IrO₂ loadings and demonstrate a seemingly synchronous increase of the disk and ring currents with the disk potential. The transit time estimated following Ref. [40] is ca. 40 ms under our experimental conditions, so the expected delay in the ring response at 10 mV s⁻¹ is below 1 mV, being indistinguishable and playing no role in the further calculation of the oxygen yield. The faradaic disc and ring currents corresponding to the bare GC disk electrode (dashed curves in Fig. 3a and b) are negligible as compared to those measured in the presence of IrO₂ even for the lowest loading of 5 μg cm⁻². The contribution of the capacitive current is essential for high catalyst loadings and, as shown below, should be taken into account when the oxygen faradaic efficiency is calculated.

Ring currents registered at a constant potential (+0.3 V) demonstrate hysteresis expanding with the catalyst loading. To understand its origin, we integrated OER currents detected in the anodic (Q_A) and cathodic (Q_C) scans on the disc and on the ring (see Tables S2 and S3). Analysis of the obtained values (see Table S2 for the rotation rate of 900 rpm) shows that for the positive-going (anodic) scans the integrals of the current acquired at the ring (and normalized to the collection efficiency and $n = 2$) are always inferior of the integrals of the disc currents, while for the negative-going (cathodic) scans one may observe an opposite behavior (except of the highest loading of 400 μg cm⁻²), as if the lag of the current in the anodic scan is compensated by its cathodic counterpart. Such a behavior might be attributed either to a contribution

¹ The ORR on the Au ring was shown to follow a two-electron pathway, see discussion below and Fig. S5.

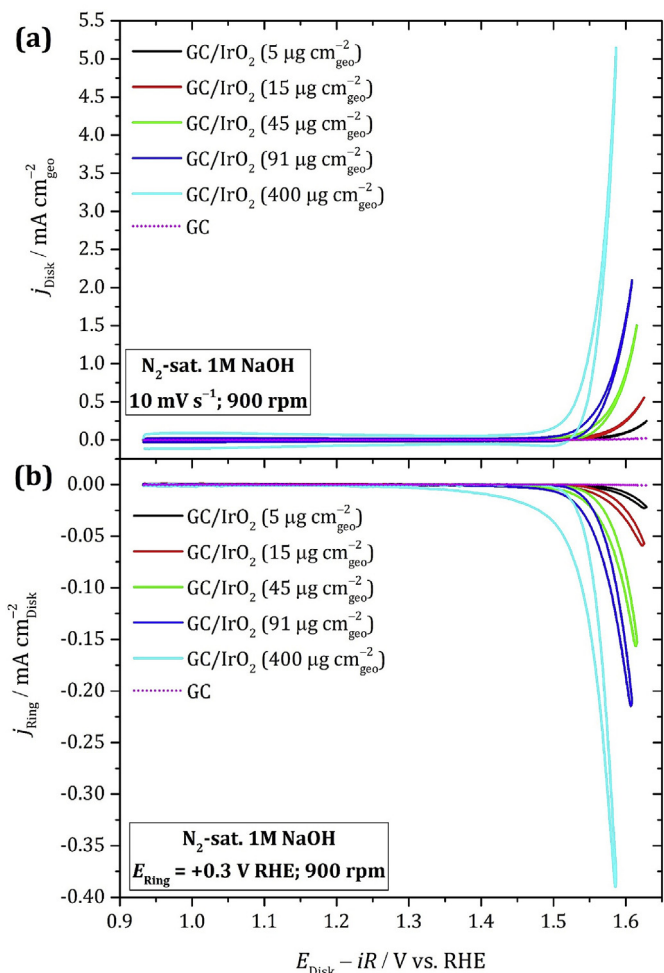


Fig. 3. RRDE CVs of GC-supported IrO₂ catalyst at 900 rpm and 10 mV s⁻¹ in N₂-saturated 1 M NaOH for various catalyst loadings: (a) disk currents; (b) ring currents at E_{Ring} = 0.3 V. All ring currents are corrected for background ring currents (reduction of oxygen traces).

of a slow chemical step to the OER as discussed e.g. in Refs. [33,41], or to complications caused by the gas evolution during the OER. In order to check on that we performed RRDE measurements at a higher rotation rate of 2500 rpm (see Table S3 and Fig. S7). Shrinking the hysteresis with the increase of the rotation rate (Fig. S7) accompanied by a diminution of the difference between the integrals of Q_A and Q_C at the ring support the second hypothesis. Probably O₂ bubbles are formed in the pores of the catalyst, from which O₂ slowly dissolves and diffuses, resulting in a decrease of the O₂ collection efficiency during the positive-going scan, while O₂ diffusion from the catalyst pores during the negative-going scan leads to an increase in the O₂ collection efficiency. Note that disc currents (both in positive- and in negative-going scans) and ring currents of the positive-going scans demonstrate negligible influence of the rotation rate and these were the anodic scans which we used for the calculation of the oxygen faradaic efficiency. The latter was calculated as $(4/2) i_{\text{Ring}} / (N i_{\text{Disk}})$, where $(4/2)$ is the ratio of the number of electrons transferred in the OER at the disk electrode and in the ORR at the ring electrode, i_{Ring} and i_{Disk} are the ring and disk currents respectively, and N is the ring collection efficiency. Two-electron ORR on the gold ring electrode was concluded from the ORR waves in the O₂-saturated 1 M NaOH solution at various electrode rotation rates (Fig. S5). The same number of electrons was

reported earlier for polycrystalline gold in alkaline solutions [42,43]. Dedicated experiments with a H₂O₂ solution (Fig. S5) confirmed that it is not reduced at the gold ring electrode at the applied potential of 0.3 V vs. RHE in 1 M NaOH.

Fig. 4 shows faradaic efficiency (panel c) along with the mass-normalized disc and ring currents acquired using the RRDE setup for various IrO₂ loadings on the disc.² Disk (Fig. 4a) as well as ring currents (Fig. 4b) merge for all loadings under study within 12% accuracy. We can conclude that the OER mass activity is independent of the catalyst loading in the studied intervals of loadings and potentials. However this conclusion cannot be straightforwardly extended to prolonged potentiostatic polarizations. At longer times, higher loadings and more positive potentials the OER currents may decrease due to the surface blocking by oxygen bubbles [44].

If *iR*-correction is not applied, one can mistakenly conclude that the mass activity decreases with the loading because the Ohmic drop increases with the current. One cannot exclude that some loading dependences reported earlier originate from an insufficient *iR*-correction. The OER activities and Tafel slopes determined in this work are compared with the literature data in Table S4 and demonstrate reasonable agreement with the data for IrO₂ in alkaline solutions, the activity being surely lower than that measured in acid media. Since often the real surface area is not documented, we considered activities normalized either to the catalyst mass or to pseudocapacitance.

The oxygen faradaic efficiency can be calculated with a reasonable accuracy for the potential interval from ca. 1.53–1.63 V (Fig. 4c) and increases abruptly from 0 to ca. 50%, and then increases more slowly up to ca. 60% for the highest loading and up to ca. 80% for other loadings. Similar efficiency increase with the disk potential was observed in Ref. [22]. Low apparent O₂ efficiency observed at the OER “onset” seems to have several origins. First of all, at low OER currents, pseudocapacitive currents contribute significantly to the measured currents (note that for electrochemically fabricated Ir oxides pseudocapacitance is much higher than for the thermal rutile-type IrO₂). This is confirmed by comparing faradaic efficiencies before and after capacity correction (Fig. S8). In the absence of this correction the values of the OER efficiency obtained under potentiodynamic conditions can be considered only for sufficiently high potentials, like in Refs. [23] and [24]. The second reason for the low OER efficiency at low OER currents is likely to be related to the slow O₂ removal from the catalyst layer discussed above. Mechanistic effects due to slow chemical step(s) cannot be fully excluded but must be confirmed using non-porous OER electrodes.

To avoid the pseudocapacity contribution we applied the RRDE technique also under potentiostatic conditions. Chronoamperometric RRDE transients acquired following a potential step from 0.93 to 1.63 V s are shown in Fig. 5 for certain loadings. The ring was held at +0.3 V during the whole experiment (Fig. 5b). Under this mode the *iR*-correction was not applied because its absence could not affect the calculation of the oxygen faradaic efficiency. In contrast to the data obtained under potentiodynamic conditions the faradaic efficiency at a constant disc potential approaches ca. 95% for the lowest loading under study (Fig. 5c), but for higher loadings the efficiency decreases with time, the higher the loading the faster the efficiency decay. The efficiency fall is obviously due to the decay of ring currents (Fig. 5b), which is faster than that of disc currents (Fig. 5a) and most probably originates from the oxygen bubble generation. At high loadings (i.e. at high disk currents) one

² Disc currents were capacity-corrected by averaging positive- and negative-going currents at each potential.

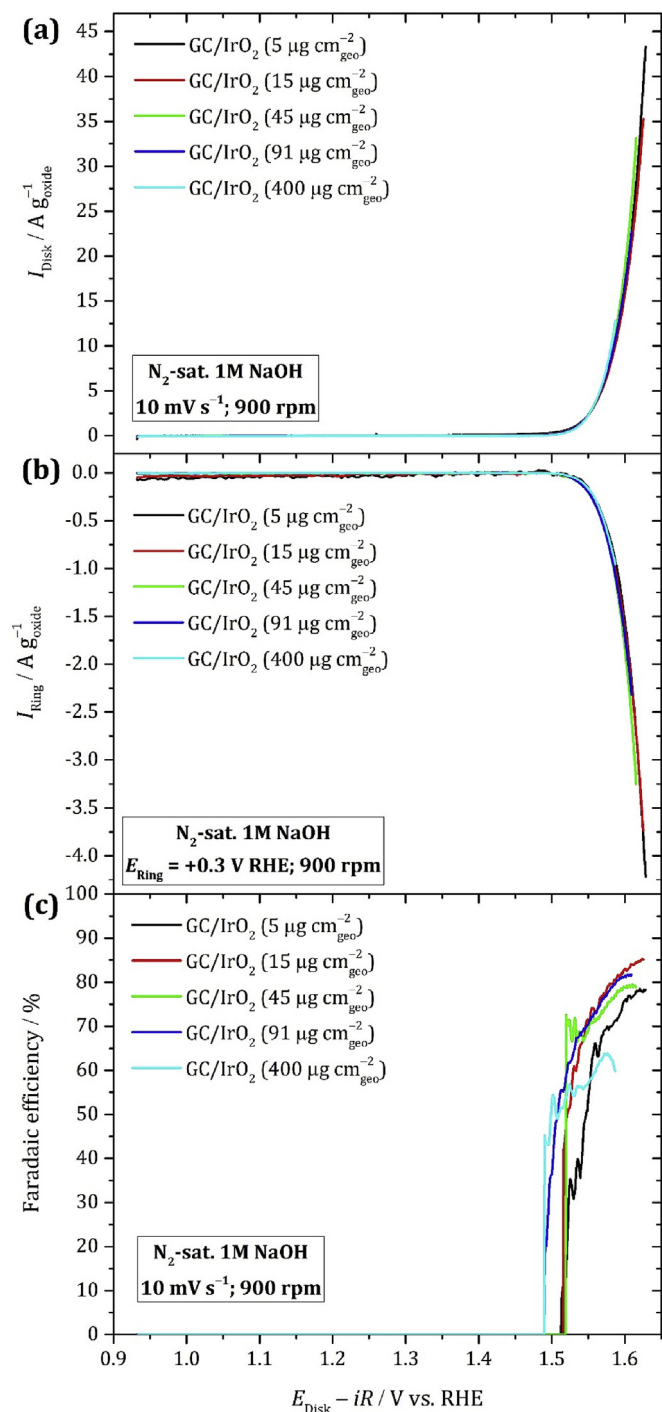


Fig. 4. RRDE CVs of GC-supported IrO₂ catalyst at 900 rpm and 10 mV s⁻¹ in N₂-saturated 1 M NaOH normalized to the catalyst loadings after GC- and capacity correction: (a) disk currents; (b) ring currents at $E_{\text{Ring}} = 0.3$ V; (c) oxygen faradaic efficiency.

can observe numerous small bubbles gathering in the vicinity of the disk-ring gap. Apparently, these oxygen bubbles block transfer of dissolved oxygen from the disk to the ring in agreement with what has been assumed in Refs. [22–24]. To confirm this hypothesis, we recorded the transients for the electrode with the highest oxide loading with a number of manual interruptions: the electrode was pulled out from time to time to remove oxygen bubbles mechanically (Fig. 6). While the transient at the disc (Fig. 6a) slowly decays

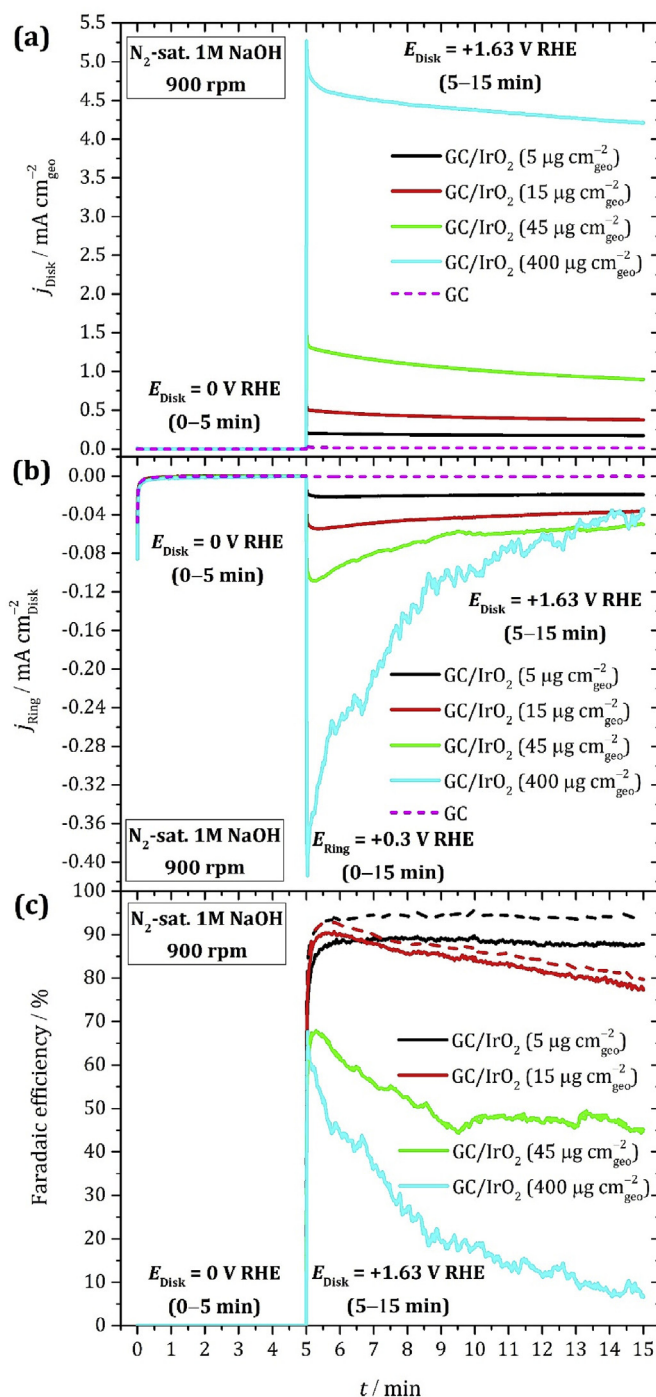


Fig. 5. RRDE transients of GC-supported IrO₂ catalyst at 900 rpm in N₂-saturated 1 M NaOH for various catalyst loadings following a potential step from 0.93 to 1.63 V (at $t = 5$ min): (a) disk currents; (b) ring currents at $E_{\text{Ring}} = 0.3$ V; (c) oxygen faradaic efficiency calculated before (solid lines) and after (dashed lines) GC-correction. Ring currents are corrected to the background ring currents.

after each interruption, the ring currents (Fig. 6b) increase and approach their initial values. Oxygen faradaic efficiency drops down sharply with time but increases again after each interruption for the bubble removal.

Unavoidable oxygen bubble formation at high OER currents restricts the RRDE applicability to quantify the oxygen evolution. Bubbles can appear after saturation of solution with evolving oxygen, but fortunately aqueous solutions tend to oxygen

supersaturation [45], and one can expect certain delay of the bubble formation. Namely, 10–15-fold oxygen supersaturation was observed in a 5.8 M KOH solution [46] and 7–120-fold supersaturation was reported for a 2 M NaOH solution [47]. Moreover, the supersaturation increases with the OER current density [47]. However it is hardly possible to use this information for any quantitative estimates because of specific features of the local supersaturation for porous electrode layers. In any case low loadings

favor the applicability of RRDE in a wider interval of the OER overpotentials (current densities). To determine oxygen efficiency correctly, it is necessary to eliminate the capacitive current contribution or (better) to study the OER with the RRDE under potentiostatic conditions.

The critical disk current density at which the oxygen bubble formation starts to affect the measured OER efficiency can be estimated from Fig. 5 as ca. $0.45 \text{ mA cm}^{-2}_{\text{geo}}$. This critical current density value likely depends on the microstructure and porosity of the catalyst layer. Therefore, quantitative application of the RRDE for the OER investigation requires determination of the critical current value for each catalyst type as a function of the catalyst loading.

3.3. RRDE investigation of the oxygen evolution on the perovskite/carbon mixtures

$\text{La}_{1-x}\text{Sr}_x\text{Mn}_{0.5}\text{Co}_{0.5}\text{O}_{3-\delta}$, $x = 0.25$ and 0.5 perovskites were used as OER catalysts to check the oxygen faradaic efficiency in the presence of a carbon binder. In this work we applied pyrolytic carbon of the Sibunit family which is known for its high stability against electrochemical corrosion [48]. To minimize the oxygen bubble generation we applied a low perovskite/carbon loading ($15/15 \mu\text{g cm}^{-2}$). The pseudocapacitances of the $\text{La}_{0.5}\text{Sr}_{0.5}\text{Mn}_{0.5}\text{Co}_{0.5}\text{O}_{3-\delta}$ and $\text{La}_{0.75}\text{Sr}_{0.25}\text{Mn}_{0.5}\text{Co}_{0.5}\text{O}_{3-\delta}$ estimated from CVs in the 0.93 – 1.03 V potential window after correction for the Sibunit carbon contribution were equal to ca. 8 and 15 F g^{-1} respectively.

Fig. 7 shows *iR*- and capacity-corrected RRDE CVs for the Sibunit and perovskite/Sibunit mixtures. Anodic currents for the perovskite/Sibunit mixtures are much higher than those observed for bare Sibunit carbon (Fig. 7a), and along with the oxygen evolution may comprise contributions from the electrochemical corrosion of both carbon and oxide components. Oxygen generation at the disc is confirmed by the appearance of oxygen reduction current at the ring (Fig. 7b). The oxygen faradaic efficiency (Fig. 7c) for perovskite/carbon mixtures obtained under galvanodynamic mode is similar to the efficiency observed for carbon-free IrO_2 catalysts with not too high loadings (ca. 70%).

The oxygen faradaic efficiency for bare Sibunit carbon is also high (ca. 70%), which is not surprising for alkaline solutions. Indeed, according to Ref. [49] anodic polarization of a graphite electrode in acid electrolytes at 20°C mostly results in its oxidation giving rise to 90–95% of CO_2 , 4% of CO and 1–6% of O_2 at pH 0.85–10 and 1.4–2 V vs. NHE, whereas in alkaline electrolytes the same graphite anode gives rise to 10% of CO_2 , 1% of CO and 89% of O_2 at pH 13–14 and 1.1–1.3 V vs. NHE. With an increase of the anodic polarization to 1.6 V vs. NHE (ca. 2.4 V vs. RHE) the amount of O_2 decreases to 60%. The oxygen faradaic efficiency on carbon strongly depends on the carbon nature. Thus Zagudaeva et al. [50] applied a RRDE to investigate the OER efficiency on the so-called “anisotropic” pyrolytic carbon with high degree of graphitization and on the “isotropic” disordered carbon. The former demonstrated the OER efficiency of ca. 50% in 0.1 M KOH, while for the latter this quantity was ca. 5%. In 0.05 M H_2SO_4 solution no oxygen reduction current was observed for both of these carbon materials at the ring of the RRDE suggesting close to zero OER efficiency.

RRDE transients for Sibunit carbon and perovskite/Sibunit mixtures are shown in Fig. 8. Like for the IrO_2 catalyst, the ring current (Fig. 8b) for the mixture with the highest activity ($\text{La}_{0.75}\text{Sr}_{0.25}\text{Mn}_{0.5}\text{Co}_{0.5}\text{O}_{3-\delta}$) decreases faster than the disk current (Fig. 8a), with corresponding decrease of the oxygen faradaic efficiency (Fig. 8c) with time due to the formation of oxygen bubbles. The faradaic efficiency for the less active $\text{La}_{0.5}\text{Sr}_{0.5}\text{Mn}_{0.5}\text{Co}_{0.5}\text{O}_{3-\delta}$ remains constant and equal to $100 \pm 5\%$. Currents originating from

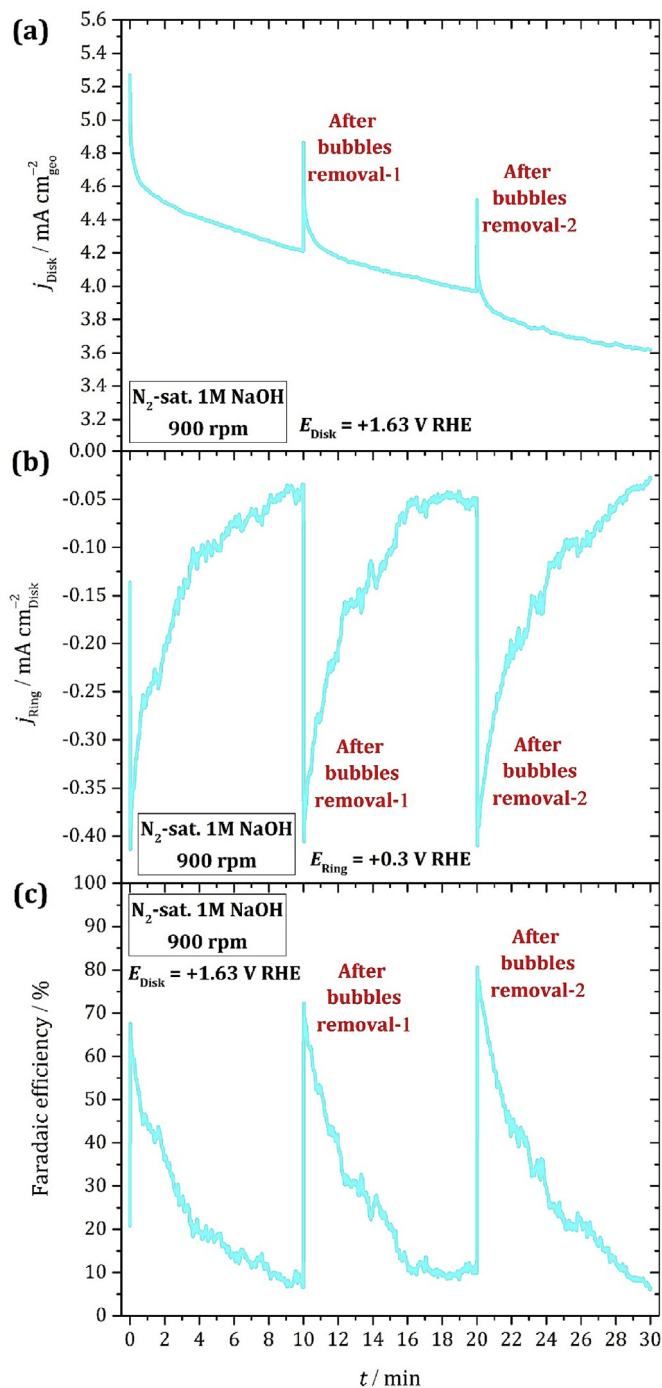


Fig. 6. RRDE transients for the GC-supported IrO_2 catalyst with $400 \mu\text{g cm}^{-2}_{\text{geo}}$ loading at 900 rpm in N_2 -saturated 1 M NaOH following a potential step from 0.93 to 1.63 V ($t=0$ min, polarization at 0.93 V is not shown here): (a) disk currents; (b) ring currents at $E_{\text{ring}} = 0.3 \text{ V}$; (c) oxygen faradaic efficiency. The RRDE was removed from the cell at $t = 10$ and 20 min to remove bubbles (see text for details).

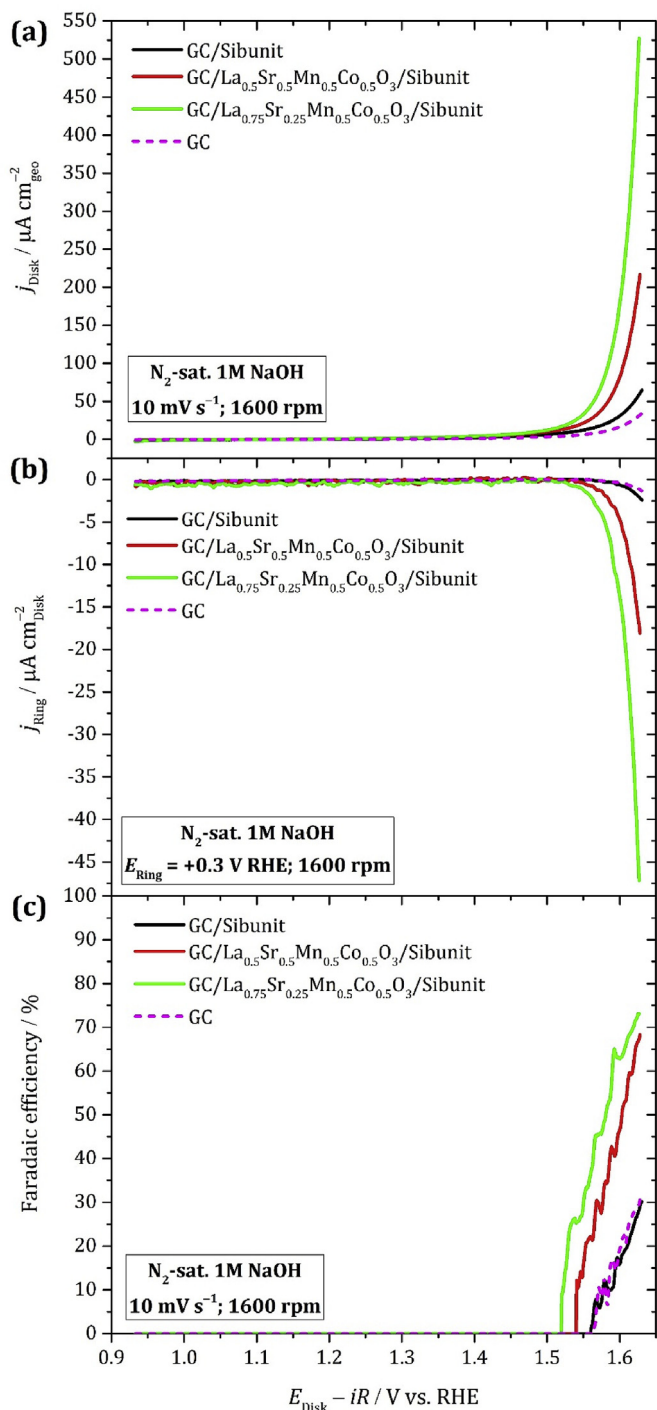


Fig. 7. RRDE CVs of GC-supported Sibunit carbon and mixtures of La_{0.5}Sr_{0.5}Mn_{0.5}Co_{0.5}O₃/Sibunit and La_{0.75}Sr_{0.25}Mn_{0.5}Co_{0.5}O₃/Sibunit at 1600 rpm and 10 mV s^{-1} in N₂-saturated 1 M NaOH with Sibunit and catalyst loadings of $15 \mu\text{g cm}^{-2}_{\text{geo}}$: (a) disk currents; (b) ring currents at $E_{\text{Ring}} = 0.3 \text{ V}$. All ring currents were corrected for the background ring currents (oxygen traces reduction).

the GC substrate also contribute to the uncertainty since at low catalyst loadings the GC surface may be partially exposed to the electrolyte. Correction of the disc current to the GC contribution results in an overestimation of the faradaic efficiency (102%), while without correction the latter is equal to ca. 97%.

Thus, using the RRDE method under conditions of its applicability for gas evolving reactions, we observed very high oxygen

faradaic efficiencies for the perovskite oxide/Sibunit mixtures suggesting that the contribution of the electrode (either carbon or metal oxide) corrosion under our experimental conditions hardly exceeds the experimental error. The upper bound of the rate of corrosion of the Sibunit binder was estimated as ca. $0.6 \pm 0.2 \text{ A g}^{-1}$ or $0.7 \pm 0.3 \mu\text{A cm}^{-2}_{\text{BET}}$ (at room temperature and $t = 15 \text{ min}$) and

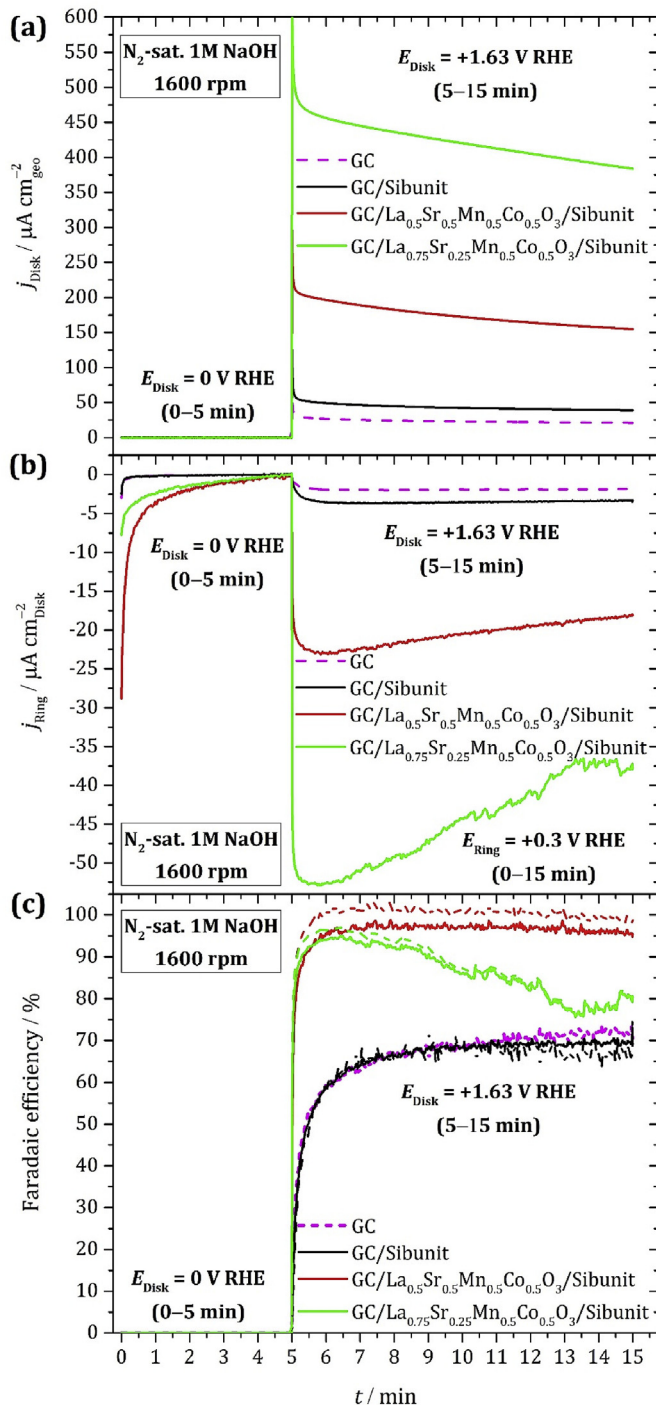


Fig. 8. RRDE transients of GC-supported Sibunit carbon and mixtures of La_{0.5}Sr_{0.5}Mn_{0.5}Co_{0.5}O₃/Sibunit and La_{0.75}Sr_{0.25}Mn_{0.5}Co_{0.5}O₃/Sibunit at 1600 rpm in N₂-saturated 1 M NaOH with Sibunit and catalyst loadings of $15 \mu\text{g cm}^{-2}_{\text{geo}}$ following a potential step from 0.93 to 1.63 V (at $t = 5 \text{ min}$): (a) disk currents; (b) ring currents at $E_{\text{Ring}} = 0.3 \text{ V}$; (c) oxygen faradaic efficiency calculated before (solid lines) and after (dashed lines) GC-correction. Ring currents are corrected to the background ring currents.

does not seem to be enhanced by the presence of the metal oxide. The observed stability of the Sibunit carbon at high anodic potentials in alkaline medium makes it a promising conductive support for the alkaline OER catalysis.

Carbon-corrected OER activity of the perovskites can be determined using Fig. 8 and at 1.6 V is equal to ca. 9.8 A g^{-1} or $96 \mu\text{A cm}^{-2}_{\text{BET}}$ for $\text{La}_{0.75}\text{Sr}_{0.25}\text{Mn}_{0.5}\text{Co}_{0.5}\text{O}_{3-\delta}$ and ca. 3.4 A g^{-1} or $60 \mu\text{A cm}^{-2}_{\text{BET}}$ for $\text{La}_{0.5}\text{Sr}_{0.5}\text{Mn}_{0.5}\text{Co}_{0.5}\text{O}_{3-\delta}$. These values are comparable with the OER activities of $\text{Mn}_x\text{Co}_{3-x}\text{O}_4$ spinels and are much higher than the OER activities of some Mn,Co-based perovskites (Table S5).

4. Conclusions

We tested the applicability of the RRDE for the quantitative determination of the oxygen evolution efficiency and activity using model IrO_2 system. The necessary steps of the procedure are *iR*-correction, correction for capacitive contribution, and examination of the current limit which allows to avoid bubble formation. The RRDE technique can be applied in a wider interval of overvoltages if one uses lower catalyst loadings. However, for low loadings the accuracy starts to decrease because of the uncertainties related to the correction for the support contribution.

We applied the RRDE to quantify the oxygen efficiency for $\text{La}_{0.5}\text{Sr}_{0.5}\text{Mn}_{0.5}\text{Co}_{0.5}\text{O}_{3-\delta}$ and $\text{La}_{0.75}\text{Sr}_{0.25}\text{Mn}_{0.5}\text{Co}_{0.5}\text{O}_{3-\delta}$ perovskites. Both were studied with the addition of pyrolytic carbon of the Sibunit family [34] in 1:1 ratio (on the weight basis). We conclude that under the conditions of the RRDE applicability the OER faradaic efficiency is close to 100% suggesting that carbons of the Sibunit family are relatively stable to corrosion in alkaline electrolytes, at least at room temperature and short electrolysis times. Contribution of Sibunit corrosion to the overall current seems to be within the accuracy of the RRDE method.

Acknowledgements

The authors are indebted to Li Wang of DLR (Stuttgart, Germany), P.A. Simonov (Novosibirsk, Russia) and Tokuyama Company (Japan) for supplying metallic iridium nanoparticles, Sibunit carbon and alkaline ionomer, respectively. Viktoriia Saveleva is gratefully acknowledged for determining the IrO_2 specific surface area, Denis M. Antipin for the synthesis of $\text{La}_{1-x}\text{Sr}_x\text{Mn}_{0.5}\text{Co}_{0.5}\text{O}_{3-\delta}$, $x = 0.25$ and 0.5 perovskites, and Alexander Ye. Baranchikov for the BET and SEM characterization of perovskites. Financial support from the National Center for Scientific Research, France and Russian Foundation for Basic Research, Russia within a joint ERA.NET.RUS project (NANO-MORF, CNRS ID 270, RFBR, Russia ID 16-53-76014) is gratefully appreciated. French Embassy in Russia for Vernadsky PhD scholarship to I.F. is specially acknowledged.

Appendix A. Supplementary data

Supplementary data related to this article can be found at <https://doi.org/10.1016/j.electacta.2018.08.056>.

References

- [1] X. Li, X. Hao, A. Abudula, G. Guan, Nanostructured catalysts for electrochemical water splitting: current state and prospects, *J. Mater. Chem. A* 4 (2016) 11973.
- [2] M. Tahir, L. Pan, F. Idrees, X. Zhang, L. Wang, J.-J. Zou, Z.L. Wang, Electrocatalytic oxygen evolution reaction for energy conversion and storage: a comprehensive review, *Nano Energy* 37 (2017) 136.
- [3] N.-T. Suen, S.-F. Hung, Q. Quan, N. Zhang, Y.-J. Xu, H.M. Chen, Electrocatalysis for the oxygen evolution reaction: recent development and future perspectives, *Chem. Soc. Rev.* 46 (2017) 337.
- [4] G. Chen, S.R. Bare, T.E. Mallouk, Development of supported bifunctional electrocatalysts for unitized regenerative fuel cells, *J. Electrochem. Soc.* 149 (2002) A1092.
- [5] S. Cherevko, S. Geiger, O. Kasian, N. Kulyk, J.-Ph. Grote, A. Savaan, B.R. Shrestha, S. Merzlikin, B. Breitbach, A. Ludwig, K.J.J. Mayrhofer, Oxygen and hydrogen evolution reactions on Ru, RuO_2 , Ir, and IrO_2 thin film electrodes in acidic and alkaline electrolytes: a comparative study on activity and stability, *Catal. Today* 262 (2016) 170.
- [6] S. Malkhandi, P. Trinh, A.K. Manohar, K.C. Jayachandrababu, A. Kindler, G.K. Surya Prakash, S.R. Narayanan, Electrocatalytic activity of transition metal oxide-carbon composites for oxygen reduction in alkaline batteries and fuel cells, *J. Electrochem. Soc.* 160 (2013) F943.
- [7] R. Mohamed, X. Cheng, E. Fabbri, P. Levecque, R. Kötz, O. Conrad, T.J. Schmidt, Electrocatalysis of perovskites: the influence of carbon on the oxygen evolution activity, *J. Electrochem. Soc.* 162 (2015) F579.
- [8] W.G. Hardin, J.T. Mefford, D.A. Slanac, B.B. Patel, X. Wang, S. Dai, X. Zhao, R.S. Ruoff, K.P. Johnston, K.J. Stevenson, Tuning the electrocatalytic activity of perovskites through active site variation and support interactions, *Chem. Mater.* 26 (2014) 3368.
- [9] X. Liu, H. Jia, Z. Sun, H. Chen, P. Xu, P. Du, Nanostructured copper oxide electrodeposited from copper(II) complexes as an active catalyst for electrocatalytic oxygen evolution reaction, *Electrochem. Commun.* 46 (2014) 1.
- [10] C. Xiao, Y. Li, X. Lu, C. Zhao, Bifunctional porous $\text{NiFe/NiCo}_2\text{O}_4/\text{Ni}$ foam electrodes with triple hierarchy and double synergies for efficient whole cell water splitting, *Adv. Funct. Mater.* 26 (2016) 3515.
- [11] S.J. Ashton, Differential electrochemical mass spectrometry, in: *Design, Construction and Research Application of a Differential Electrochemical Mass Spectrometer (DEMS)*, Springer, Berlin, Heidelberg, 2012, pp. 9–24.
- [12] E. Pizzutilo, S. Geiger, J.-P. Grote, A. Mingers, K.J.J. Mayrhofer, M. Arenz, S. Cherevko, On the need of improved accelerated degradation protocols (ADPs): examination of platinum dissolution and carbon corrosion in half-cell tests, *J. Electrochem. Soc.* 163 (2016) F1510.
- [13] K. Macounova, M. Makarova, J. Jirkovsky, J. Franc, P. Krtil, Parallel oxygen and chlorine evolution on $\text{Ru}_{1-x}\text{Ni}_x\text{O}_{2-y}$ nanostructured electrodes, *Electrochim. Acta* 53 (2008) 6126.
- [14] A.R. Zeradjanin, N. Menzel, W. Schuhmann, P. Strasser, On the faradaic selectivity and the role of surface inhomogeneity during the chlorine evolution reaction on ternary Ti–Ru–Ir mixed metal oxide electrocatalysts, *Phys. Chem. Chem. Phys.* 16 (2014) 13741.
- [15] H.M.A. Amin, H. Baltruschat, How many surface atoms in Co_3O_4 take part in oxygen evolution? Isotope labeling together with differential electrochemical mass spectrometry, *Phys. Chem. Chem. Phys.* 19 (2017) 25527.
- [16] A. Grimaud, O. Diaz-Morales, B. Han, W.T. Hong, Y.-L. Lee, L. Giordano, K.A. Stoerzinger, M.T.M. Koper, Y. Shao-Horn, Activating lattice oxygen redox reactions in metal oxides to catalyze oxygen evolution, *Nat. Chem.* 9 (2017) 457.
- [17] A. Minguzzi, M.A. Alpuche-Aviles, J. Rodríguez-López, S. Rondinini, A.J. Bard, Screening of oxygen evolution electrocatalysts by scanning electrochemical microscopy using a shielded tip approach, *Anal. Chem.* 80 (2008) 4055.
- [18] X. Chen, A.J.R. Botz, J. Masa, W. Schuhmann, Characterisation of bifunctional electrocatalysts for oxygen reduction and evolution by means of SECM, *J. Solid State Electrochem.* 20 (2016) 1019.
- [19] C.C.L. McCrory, S. Jung, J.C. Peters, T.F. Jaramillo, Benchmarking heterogeneous electrocatalysts for the oxygen evolution reaction, *J. Am. Chem. Soc.* 135 (2013) 16977.
- [20] G. Li, L. Anderson, Y. Chen, M. Pan, P.-Y.A. Chuang, New insights into evaluating catalyst activity and stability for oxygen evolution reactions in alkaline media, *Sustain. Energy Fuels* 2 (2018) 237.
- [21] Q. Gao, Ch. Ranjan, Z. Pavlovic, R. Blume, R. Schlögl, Enhancement of stability and activity of MnO_x/Au electrocatalysts for oxygen evolution through adequate electrolyte composition, *ACS Catal.* 5 (2015) 7265.
- [22] S. Drespf, F. Luo, R. Schmack, S. Kühn, M. Gliche, P. Strasser, An efficient bifunctional two-component catalyst for oxygen reduction and oxygen evolution in reversible fuel cells, electrolyzers and rechargeable air electrodes, *Energy Environ. Sci.* 9 (2016) 2020.
- [23] A.T. Swesi, J. Masud, M. Nath, Nickel selenide as a high-efficiency catalyst for oxygen evolution reaction, *Energy Environ. Sci.* 9 (2016) 1771.
- [24] Y. Qiu, L. Xin, W. Li, Electrocatalytic oxygen evolution over supported small amorphous Ni–Fe nanoparticles in alkaline electrolyte, *Langmuir* 30 (2014) 7893.
- [25] A.S. Batchellor, S.W. Boettcher, Pulse-Electrodeposited Ni–Fe (Oxy)hydroxide oxygen evolution electrocatalysts with high geometric and intrinsic activities at large mass loadings, *ACS Catal.* 5 (2015) 6680.
- [26] B.S. Yeo, A.T. Bell, Enhanced activity of gold-supported cobalt oxide for the electrochemical evolution of oxygen, *J. Am. Chem. Soc.* 133 (2011) 5587.
- [27] C.G. Morales-Guio, L. Liardet, X. Hu, Oxidatively electrodeposited thin-film transition metal (Oxy)Hydroxides as oxygen evolution catalysts, *J. Am. Chem. Soc.* 138 (2016) 8946.
- [28] L. Brossard, C. Messier, Effect of cobalt deposits on nickel substrates on the oxygen evolution reaction in KOH, *J. Appl. Electrochem.* 23 (1993) 379.
- [29] W. Hu, Y. Wang, X. Hu, Y. Zhou, S. Chen, Three-dimensional ordered macroporous IrO_2 as electrocatalyst for oxygen evolution reaction in acidic medium, *J. Mater. Chem.* 22 (2012) 6010.
- [30] Y. Lee, J. Suntivich, K.J. May, E.E. Perry, Y. Shao-Horn, Synthesis and activities of rutile IrO_2 and RuO_2 nanoparticles for oxygen evolution in acid and alkaline solutions, *J. Phys. Chem. Lett.* 3 (2012) 399.
- [31] P. Lettenmeier, L. Wang, U. Golla-Schindler, P. Gazdzicki, N.A. Cañas, M. Handl,

- R. Hiesgen, S.S. Hosseiny, A.S. Gago, K.A. Friedrich, Nanosized IrO_x–Ir catalyst with relevant activity for anodes of proton exchange membrane electrolysis produced by a cost-effective procedure, *Angew. Chem.* 55 (2016) 742.
- [32] V.A. Saveleva, L. Wang, W. Luo, S. Zafeiratos, C. Ulhaq-Bouillet, A.S. Gago, K.A. Friedrich, E.R. Savinova, Uncovering the stabilization mechanism in bimetallic ruthenium-iridium anodes for proton exchange membrane electrolyzers, *J. Phys. Chem. Lett.* 7 (2016) 3240.
- [33] V.A. Saveleva, L. Wang, D. Teschner, T. Jones, A.S. Gago, K.A. Friedrich, S. Zafeiratos, R. Schlögl, E.R. Savinova, Operando evidence for a universal oxygen evolution mechanism on thermal and electrochemical iridium oxides, *J. Phys. Chem. Lett.* 9 (2018) 3154.
- [34] Yu.I. Yermakov, V.F. Surovikin, G.V. Plaksin, V.A. Semikolenov, V.A. Likhobobov, L.V. Chuvilin, S.V. Bogdanov, New carbon material as support for catalysts, *React. Kinet. Catal. Lett.* 33 (1987) 435.
- [35] A.S. Ryabova, F.S. Napol'skiy, T. Poux, S.Ya. Istomin, A. Bonnefont, D.M. Antipin, A.Ye. Baranchikov, E.E. Levin, A.M. Abakumov, G. Kéranguéven, E.V. Antipov, G.A. Tsirlina, E.R. Savinova, Rationalizing the influence of the Mn(IV)/Mn(III) red-ox transition on the electrocatalytic activity of manganese oxides in the oxygen reduction reaction, *Electrochim. Acta* 187 (2016) 161.
- [36] M.E.G. Lyons, S. Floquet, Mechanism of oxygen reactions at porous oxide electrodes. Part 2—oxygen evolution at RuO₂, IrO₂ and Ir_xRu_{1-x}O₂ electrodes in aqueous acid and alkaline solution, *Phys. Chem. Chem. Phys.* 13 (2011) 5314.
- [37] G.C. da Silva, N. Perini, E.A. Ticianelli, Effect of temperature on the activities and stabilities of hydrothermally prepared IrO_x nanocatalyst layers for the oxygen evolution reaction, *Appl. Catal. B Environ.* 218 (2017) 287.
- [38] S. Geiger, O. Kasian, B.R. Shrestha, A.M. Mingers, K.J.J. Mayrhofer, S. Cherevko, Activity and stability of electrochemically and thermally treated iridium for the oxygen evolution reaction, *J. Electrochem. Soc.* 163 (2016) F3132.
- [39] C. Angelinetta, S. Trasatti, L.J.D. Atanasoska, Z.S. Minevski, R.T. Atanasoski, Effect of preparation on the surface and electrocatalytic properties of RuO₂ + IrO₂ mixed oxide electrodes, *Mater. Chem. Phys.* 22 (1989) 231.
- [40] A.J. Bard, L.R. Faulkner, *Electrochemical Methods: Fundamentals and Applications*, second ed., vols. 351–352, John Wiley & Sons, New York, Chichester, Weinheim, Brisbane, Singapore, Toronto, 2001, pp. 355–356.
- [41] S. Trasatti, Electrocatalysis in the anodic evolution of oxygen and chlorine, *Electrochim. Acta* 29 (1984) 1503.
- [42] R.R. Adžić, A.V. Tripković, N.M. Marković, Oxygen reduction on electrode surfaces modified by foreign metal ad-atoms: lead ad-atoms on gold, *J. Electroanal. Chem.* 114 (1980) 37.
- [43] V. Vesovic, N. Anastasijević, R.R. Adžić, Rotating disk electrode: a re-examination of some kinetic criteria with a special reference to oxygen reduction, *J. Electroanal. Chem.* 218 (1987) 53.
- [44] V.I. Rostokin, Yu.G. Chirkov, Theory of the rotating disk gas-generating porous electrode, *Elektrokhimiya* 36 (2000) 735.
- [45] H. Vogt, On the supersaturation of gas in the concentration boundary layer of gas evolving electrodes, *Electrochim. Acta* 25 (1980) 527.
- [46] E.A. Khomskaya, A.S. Kolosov, Determination of the degree of supersaturation with oxygen of a KOH solution by the rotating disk-ring electrode method, *Elektrokhimiya* 6 (1970) 256.
- [47] V.G. Nefedov, Kinetics of formation of flat gas-bubble nuclei on electrodes, *Elektrokhimiya* 33 (1997) 815.
- [48] O.V. Cherstiouk, A.N. Simonov, N.S. Moseva, S.V. Cherepanova, P.A. Simonov, V.I. Zaikovskii, E.R. Savinova, Microstructure effects on the electrochemical corrosion of carbon materials and carbon-supported Pt catalysts, *Electrochim. Acta* 55 (2010) 8453.
- [49] N.D. Vyet, D.V. Kokoulina, L.I. Krishtalik, Investigation of electrochemical oxidation of a graphite anode. III. Composition of anodic products as affected by the state of anode surface and its polarization characteristics, *Elektrokhimiya* 8 (1972) 384.
- [50] N.M. Zagudaeva, K.A. Radyushkina, M.R. Tarasevich, Development of a method for investigation of the corrosion of carbon materials with the use of a disk-ring electrode, *Elektrokhimiya* 21 (1985) 1406.